Magnetic field induced one-magnon Raman scattering in the magnon Bose-Einstein condensation phase of $TlCuCl_3$

Haruhiko Kuroe,* Kouhei Kusakabe, Akira Oosawa, and Tomoyuki Sekine
Department of Physics, Sophia University, 7-1 Kioi-cho, Chiyoda-ku, Tokyo 102-8554, Japan

Fumiko Yamada and Hidekazu Tanaka
Department of Physics, Tokyo Institute of Technology, Oh-okayama, Meguro-ku, Tokyo 152-8551, Japan

Masashige Matsumoto
Department of Physics, Shizuoka University, 836 Oya, Shizuoka 422-8529, Japan
(Received 2 January 2008; published 9 April 2008; corrected 10 April 2008)

We report the observation of the A_g-symmetric one-magnon Raman peak in the magnon Bose-Einstein condensation phase of $TlCuCl_3$. Its Raman shift traces the one-magnon energy at the magnetic Γ point, and its intensity is proportional to the squared transverse magnetization. The appearance of the one-magnon Raman scattering originates from the exchange magnon Raman process and reflects the change of the magnetic-state symmetry. By using the bond-operator representation, we theoretically clarify the Raman selection rules, which are consistent with the experimental results.

DOI: 10.1103/PhysRevB.77.134420 PACS number(s): 78.30.−j, 75.10.Jm

I. INTRODUCTION

Currently, many physicists are examining the Bose-Einstein condensation (BEC) of atoms in ultracooled dilute gases and, in particular, the BEC of magnons. The latter, which is the magnetic field induced quantum phase transition to the magnon BEC phase, has been reported in $S=1/2$ antiferromagnets with a spin gap, such as $KCuCl_3$, $TlCuCl_3$,[1–4] $BaCuSi_2O_6$,[5] and $Pb_2V_3O_9$.[6] The change of the magnon dispersion relation in $TlCuCl_3$ through the magnon BEC phase transition at $H_c \sim 6$ T has been observed by inelastic neutron scattering[7] and has been explained by using the bond-operator representation.[8] One of the characteristic features of the magnon BEC phase is the formation of massless excitation, i.e., the Goldstone mode at the magnetic Γ point, which indicates the spontaneous breaking of the continuous symmetry. However, the details of the magnon excitations, especially their symmetries, have not yet been established. Raman scattering is a powerful tool to study phase transitions. Because the magnon Raman process is sensitive to the symmetries of the ground and excited states,[9] Raman-scattering measurement above H_c presents a great opportunity to study the change of the ground and excited states through the magnon BEC phase transition.

This paper reports the observation of one-magnon Raman scattering originating from changes of the ground and excited states through the magnon BEC phase transition. This study focused on $TlCuCl_3$ where the magnon excitations and magnetic parameters below and above H_c have been studied in detail.[7,8] First, we show our experimental results above H_c. We then construct the microscopic theory of one-magnon Raman scattering in the exchange magnon Raman process by using the bond-operator representation, which can clearly explain the experimental results. Based on our results, the Raman selection rule will be clarified.

II. EXPERIMENTS

Single crystals of $TlCuCl_3$ were prepared by the vertical Bridgman method.[1] The 5145 Å line of Ar^+-ion laser polarized along the (201) axis was incident on the (010) cleavage surface. We set the samples in the cryostat under the dried N_2 or He gas atmosphere because these samples were easily damaged by the moisture in air. We placed the microscope in the vacuum chamber of superconducting magnet in order to effectively collect the scattered light. This enabled us to select good surface positions of crystals, and the effects of the direct scattering in the low-energy region were avoided. Magnetic fields of up to 10 T were applied nearly parallel to the (010) axis. The effect of a weak component of magnetic field along the (201) axis due to the experimental setting is negligible because the effect of the anisotropic g tensor along these directions is small.[10]

III. RESULTS

Figure 1 compares the low-temperature Raman spectrum at 9 T (above H_c of $TlCuCl_3$) to that at 0 T. At 0 T, we observed several sharp phonon peaks superimposed on the two-magnon Raman band extending from 11 cm^{-1}, i.e., twice the energy of the magnetic gap,[7] to about 120 cm^{-1}. This spectrum is consistent with the results of Refs. 11 and 12. At 9 T, we observed the Raman peak with a Lorentzian line shape, called P1, at 20 cm^{-1}. No other significant change was observed. P1 excitation has the A_g symmetry, which is obtained with the following procedures. For the incident laser polarized along the (201) axis, $\boldsymbol{E}_{\rm in}//(201)$, we measured the scattered light with polarization $\boldsymbol{E}_{\rm sc}$, which is rotated from $\boldsymbol{E}_{\rm in}$ with an angle θ. The Raman intensities are normalized so that the 137 cm^{-1} A_g-symmetric phonon peaks in each spectrum, in which the θ dependence is shown in the inset of Fig. 1, have the same intensity. The Raman intensity from the quasiparticles with A_g symmetry, including P1, is θ independent in this plot, while those with B_g symmetry, indicated by arrows, increased with increasing θ, as shown in Fig. 1.

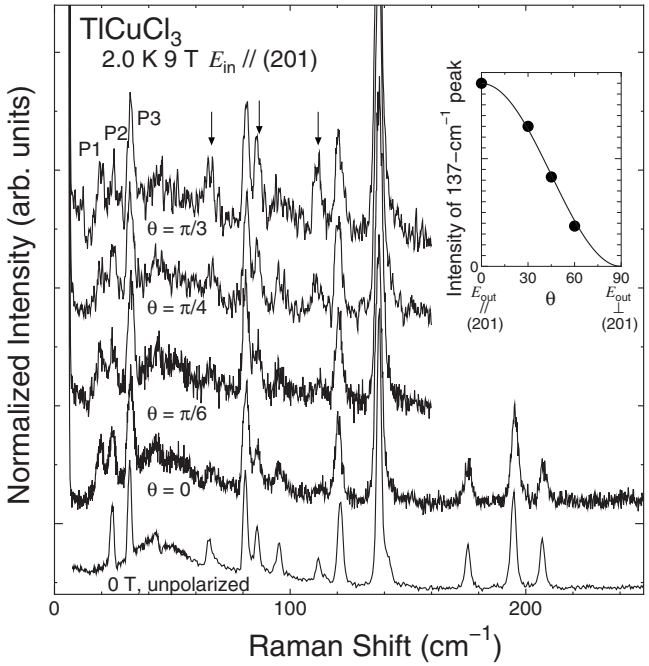

FIG. 1. Polarization characteristics of Raman spectra at 9 T. The inset shows the integrated Raman intensity of the phonon peak at 137 cm^{-1}. The arrows indicate the Raman peaks coming from the B_g phonons. The unpolarized Raman spectrum at 0 T is also shown.

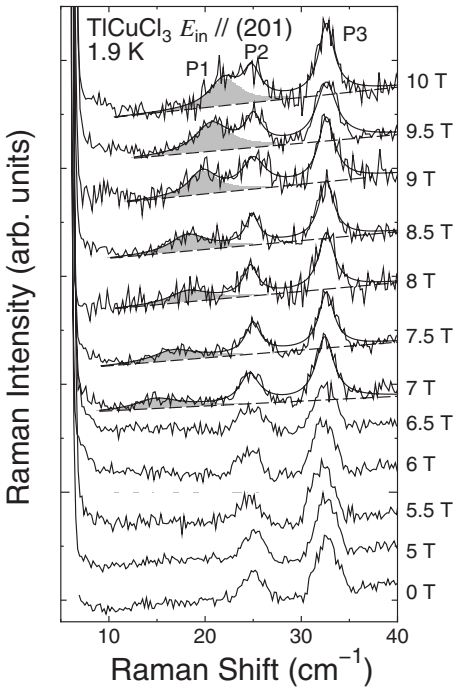

FIG. 2. Magnetic field dependence of Raman spectra in $TlCuCl_3$ at 1.9 K. The fitting curves are superimposed on the experimental data above 7 T. The details of the fitting curve (solid curves) together with the background generated by the two-magnon Raman band (dashed lines) are given in the text. The hatched areas show the component of the Raman intensity generated by P1.

Figure 2 shows the detailed magnetic field dependence of Raman spectra at 1.9 K. At 0 T, the 25 and 32 cm^{-1} phonon Raman peaks, called P2 and P3, respectively, are superimposed on the two-magnon Raman band starting at 11 cm^{-1}. P2 and P3 have the A_g symmetry as well as P1, as shown in Fig. 1. The Raman spectra below 5 T are magnetic field independent. Above 7 T, we clearly observed that the frequency and intensity of P1 strongly depended on the applied magnetic field, as denoted by the hatched areas in Fig. 2, of which the details will be explained later. Around 6 T, the increase in the Rayleigh scattering around 0 cm^{-1} suggests the quasielastic (or critical) light scattering reflecting the large magnetic specific heat around H_c as observed in several antiferromagnets or spin-Peierls system.[13–15] To quantitatively discuss the quasielastic light scattering, Raman-scattering measurements in the anti-Stokes region are necessary.

The line shapes of P1, P2, and P3 are well described by three Lorentzian curves superimposed on the background,

$$I(\omega) = \sum_{i=1}^{3} \frac{(n+1)k_i^2 \omega \Gamma_i}{(\omega^2 - \omega_i^2)^2 + (\omega \Gamma_i)^2} + \text{background}, \qquad (1)$$

where k_i, $\hbar\omega_i$, and Γ_i indicate the Raman coupling coefficient, the energy, and the half width of Pi, respectively. Here, the Bose factor $(n+1)$ can be treated as unity because the temperature is much lower than the energies of quasiparticles. The background generated by the two-magnon Raman band peaking around 50 cm^{-1} was assumed to be a linear function, as shown by the dashed lines in Fig. 2. The calculated curves reproduced the observed data well. We show the Raman intensity generated by P1 [the term related to the subscript $i=1$ in Eq. (1)] on the linear background as the hatched area in Fig. 2. Around H_c, we could not distinguish P1 from the two-magnon Raman band because of its weak intensity.

Figure 3(a) shows the peak energies $\hbar\omega_1$ and $\hbar\omega_2$ as functions of magnetic field together with the calculated one-magnon energy $E_{g\alpha}(\boldsymbol{Q})$ $(\alpha=-,0,+)$ with the wave vector $\boldsymbol{Q}=(0,0,2\pi)$,[8,16] where the magnetic gap is closed.[3,17] One can see that $\hbar\omega_1$ below 10 T agrees with $E_{g-}(\boldsymbol{Q})$ within experimental accuracy. Figure 3(b) shows the squared Raman coupling coefficient $k^2=k_1^2/k_3^2$, which is proportional to the integrated Raman intensity of P1. Here, we normalized k_1^2, which is proportional to the area hatched in Fig. 2, by k_3^2 to correct errors due to the small deviations of optic alignment. The errors of k^2 are similar to the symbol size in Fig. 3(b). For comparison, we show the magnetic field dependences of squared transverse magnetization M_{xy}^2 (Ref. 3) and squared longitudinal magnetization M_z^2 (Ref. 18) together with their calculated values.[8] One can see that the magnetic field dependence of Raman intensity is well scaled to the former.

IV. DISCUSSION

First, we discuss the origin of P1. Judging from the polarization characteristics, the scattering process of P1 comes from the exchange magnon Raman scattering, as proposed by Fleury and Loudon,[9] which usually creates the broad two-magnon Raman band with A_g symmetry reported at zero magnetic field.[11,12] Because the two-magnon Raman band at

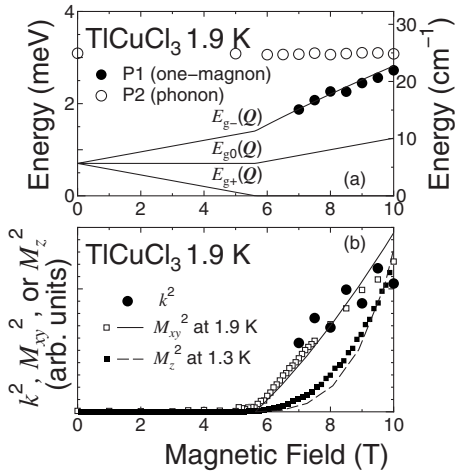

FIG. 3. (a) Magnetic field dependence of one-magnon (filled circles) and phonon (empty circles) energies together with that of one-magnon energies calculated in Refs. 8 and 16. (b) Magnetic field dependence of squared Raman coupling coefficient (filled circles). Squared transverse magnetization M_{xy}^2 (empty squares, Ref. 3) and squared longitudinal magnetization M_z^2 (filled squares, Ref. 18) are also plotted with the calculated values for them (a solid and a dashed curve for M_{xy}^2 and M_z^2, respectively) (Ref. 8).

9 T is almost the same as that at 0 T, as seen in Fig. 1, we do not need to consider the increase in the magnon-magnon interaction which may cause the two-magnon Raman band with a nearly Lorentzian line shape[19,20] as well as the formation of the two-magnon bound state.[21] P1 does not originate from a three-magnon process, where the thermally excited triplets play an essential role.[22,23] The three-magnon Raman intensity, which is proportional to n at low temperatures, should be negligibly small at 1.9 K. Because P1 has a Lorentzian line shape, the one-magnon Raman scattering can be considered as the origin of P1. Hereafter, we consider the detail of the magnon Raman process by using the bond-operator representation and clarify that the one-magnon Raman scattering from the exchange magnon Raman process becomes possible in the magnon BEC phase.

The effective Raman operator $\mathcal{R}$ in the above-mentioned exchange magnon Raman process has a form given by the isotropic Heisenberg-type exchange interaction between spins $\boldsymbol{S}_i$ and $\boldsymbol{S}_j$,

$$\mathcal{R} = \sum_{i,j} \mathcal{R}_{i,j} = \sum_{i,j} F_{i,j}(\hat{\boldsymbol{E}}_{\rm in} \cdot \hat{\boldsymbol{r}}_{ij})(\hat{\boldsymbol{E}}_{\rm sc} \cdot \hat{\mathbf{r}}_{ij})\boldsymbol{S}_i \cdot \boldsymbol{S}_j, \tag{2}$$

where $\boldsymbol{r}_{ij}$ indicates the position vector between $\boldsymbol{S}_i$ and $\boldsymbol{S}_j$ and the sum runs over all the interacting spin pairs. Here, $\hat{\boldsymbol{r}} = \boldsymbol{r}/|\boldsymbol{r}|$, $\hat{\boldsymbol{E}} = \boldsymbol{E}/|\boldsymbol{E}|$, and the coefficient $F_{i,j}$ depends on the pathway of interaction between $\boldsymbol{S}_i$ and $\boldsymbol{S}_j$. $\mathcal{R}$ depends on the experimental setting through the $(\hat{\boldsymbol{E}}_{\rm in} \cdot \hat{\boldsymbol{r}}_{ij})(\hat{\boldsymbol{E}}_{\rm sc} \cdot \hat{\boldsymbol{r}}_{ij})$ term. The matrix element of $\mathcal{R}$ between the initial state $|i\rangle$ and the final one $|f\rangle$ is called the Raman tensor. The magnon Raman intensity is given as

$$\mathcal{I}^{(\rm in,sc)}(\omega) \propto |\boldsymbol{E}_{\rm in}|^2 \sum_{|f\rangle} |\langle i|\mathcal{R}|f\rangle|^2 \delta(\omega - \omega_{if}), \tag{3}$$

where $\hbar\omega_{if}$ is the excitation energy between the states $|i\rangle$ and $|f\rangle$.

We note here that $\mathcal{R}$ is *always* written by using the pure singlet operator $s_{\boldsymbol{k}}$ and the triplet operators $t_{\boldsymbol{k}\alpha}$ $(\alpha = -, 0, +)$, which annihilate the triplets with $S^z = \alpha$. We need to rewrite $\mathcal{R}$ by using the creation and annihilation operators of eigenstates in the magnon BEC phase. As discussed by Matsumoto *et al.*,[8,16] the following transformed operators based on the bond-operator representation characterize the magnon excitations in the magnon BEC phase,

$$\begin{aligned} s_{\boldsymbol{k}} &= u a_{\boldsymbol{k}} - v b_{\boldsymbol{k}+\boldsymbol{Q}+}, \\ t_{\boldsymbol{k}+} &= v f a_{\boldsymbol{k}-\boldsymbol{Q}} + u f b_{\boldsymbol{k}+} - g b_{\boldsymbol{k}-}, \\ t_{\boldsymbol{k}0} &= b_{\boldsymbol{k}0}, \\ t_{\boldsymbol{k}-} &= v g a_{\boldsymbol{k}-\boldsymbol{Q}} + u g b_{\boldsymbol{k}+} + f b_{\boldsymbol{k}-}, \end{aligned} \tag{4}$$

where the momentum-independent real-number parameters u, v, f, and g satisfy $f^2 + g^2 = u^2 + v^2 = 1$. Below H_c, $v = 0$ and one can obtain the simple relations $a_{\boldsymbol{k}} = s_{\boldsymbol{k}}$ and $b_{\boldsymbol{k}\alpha} = t_{\boldsymbol{k}\alpha}$. Above H_c, $v \neq 0$ and the operators $a_{\boldsymbol{k}-\boldsymbol{Q}}$ and $b_{\boldsymbol{k}\pm}$ are linearly combined. The mixing of $b_{\boldsymbol{k}\pm}$ and $b_{-\boldsymbol{k}\pm}^\dagger$ is treated by using the Bogoliubov transformation, as will be shown in detail later. It should be noted that the ground state does not include the $b_{\boldsymbol{k}0}$ state, which indicates that the $E_{g0}(\boldsymbol{Q})$ mode is not Raman active.

We consider the Raman operator $\mathcal{R}_{\boldsymbol{d}}$ associated with the intradimer interaction, which can be written in the reciprocal lattice space as

$$\begin{aligned} \mathcal{R}_{\boldsymbol{d}} &= F_{\boldsymbol{d}}(\hat{\boldsymbol{E}}_{\rm in} \cdot \hat{\boldsymbol{d}})(\hat{\boldsymbol{E}}_{\rm sc} \cdot \hat{\boldsymbol{d}}) \sum_{\boldsymbol{k}} \left(-\frac{3}{4} s_{\boldsymbol{k}}^\dagger s_{\boldsymbol{k}} + \sum_{\alpha} \frac{1}{4} t_{\boldsymbol{k}\alpha}^\dagger t_{\boldsymbol{k}\alpha} \right) \\ &= F_{\boldsymbol{d}}(\hat{\boldsymbol{E}}_{\rm in} \cdot \hat{\boldsymbol{d}})(\hat{\boldsymbol{E}}_{\rm sc} \cdot \hat{\boldsymbol{d}}) \Bigg[\left(\frac{1}{4} - u^2 \right) \bar{a}^2 + uv\bar{a}(b_{\boldsymbol{Q}+} + b_{\boldsymbol{Q}+}^\dagger) \\ &\quad + \sum_{\boldsymbol{k}} \left\{ \left(\frac{1}{4} - v^2 \right) b_{\boldsymbol{k}+}^\dagger b_{\boldsymbol{k}+} + \frac{1}{4} b_{\boldsymbol{k}-}^\dagger b_{\boldsymbol{k}-} + \frac{1}{4} b_{\boldsymbol{k}0}^\dagger b_{\boldsymbol{k}0} \right\} \Bigg], \end{aligned} \tag{5}$$

where $\boldsymbol{d}$ indicates the position vector between two spins forming a dimer, which is almost parallel to the (201) direction, and $F_{\boldsymbol{d}}$ originates from $F_{i,j}$. Here, we used the fact that the operator $a_{\boldsymbol{k}}$ can be treated as a uniformly condensed mean-field parameter $\bar{a}\delta_{\boldsymbol{k},0}$ (Ref. 16) and $b_{-\boldsymbol{Q}+}^\dagger = b_{\boldsymbol{Q}+}^\dagger$ at the magnetic Γ point. The term $uv\bar{a}(b_{\boldsymbol{Q}+} + b_{\boldsymbol{Q}+}^\dagger)$ in Eq. (5) gives the momentum selection rule of one-magnon Raman scattering. The parameter uv indicates the appearance of one-magnon Raman scattering only above H_c and the Raman intensity proportional to M_{xy}^2 [see Eq. (5) of Ref. 16], which is consistent with the observation, as shown in Fig. 3(b). The terms $\bar{a}^2$ and $b_{\boldsymbol{k}\alpha}^\dagger b_{\boldsymbol{k}\alpha}$ in Eq. (5) do not give one-magnon Raman scattering.

The quadratic terms of the magnetic Hamiltonian $\mathcal{H}_\pm$ in Ref. 8 can be diagonalized by using the $\alpha_{\boldsymbol{k}}^\pm$ bosonic operators which annihilate the $E_{g\pm}(\boldsymbol{k})$ modes. The ground state in the magnon BEC phase is the vacuum state for the $\alpha_{\boldsymbol{k}}^\pm$ operators. By using the bosonic commutation relations of $\alpha_{\boldsymbol{k}}^\pm$, we obtain the inverse Bogoliubov transformation as

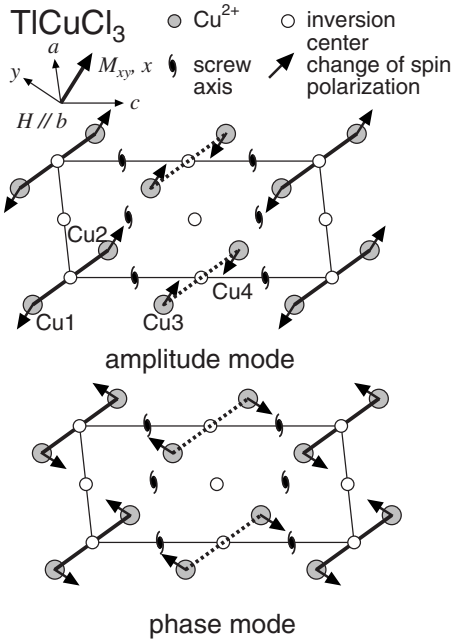

FIG. 4. Changes of spin polarizations for the amplitude and phase modes, which correspond to the ionic-vibration patterns in phonons. The solid and dashed lines indicate the dimers at the corner and center of the chemical unit cell denoted by parallelograms, respectively. Only the Cu^{2+} sites are shown with the symbols of inversion centers and screw axes. The direction of the transverse magnetization x in the magnon BEC phase is shown by a bold arrow with M_{xy} (Ref. 3). The direction y is perpendicular to x and b.

$$\begin{pmatrix} b_{k-} \\ b_{k+} \\ b^{\dagger}_{-k-} \\ b^{\dagger}_{-k+} \end{pmatrix} = \begin{pmatrix} u^{-*}_{-k-} & u^{+*}_{-k-} & -v^{-}_{k-} & -v^{+}_{k-} \\ u^{-*}_{-k+} & u^{+*}_{-k+} & -v^{-}_{k+} & -v^{+}_{k+} \\ -v^{-*}_{-k-} & -v^{+*}_{-k-} & u^{-}_{k-} & u^{+}_{k-} \\ -v^{-*}_{-k+} & -v^{+*}_{-k+} & u^{-}_{k+} & u^{+}_{k+} \end{pmatrix} \begin{pmatrix} \alpha^{-}_{k} \\ \alpha^{+}_{k} \\ \alpha^{-\dagger}_{-k} \\ \alpha^{+\dagger}_{-k} \end{pmatrix}. \tag{6}$$

The one-magnon term in Eq. (5) can be rewritten as

$$b_{Q+} + b^{\dagger}_{Q+} = (u^{-}_{Q+} - v^{-}_{Q+})^{*}\alpha^{-}_{Q} + (u^{+}_{Q+} - v^{+}_{Q+})^{*}\alpha^{+}_{Q} + \text{H . c . }, \tag{7}$$

which indicates that both the $E_{g+}(\boldsymbol{Q})$ and $E_{g-}(\boldsymbol{Q})$ modes are symmetrically allowed. These modes can be described as the mixed amplitude and phase modes which are related to the spin correlation functions along the x and y directions in Fig. 4, respectively. The amplitude mode changes the amplitudes of M_{xy} without changing their directions, whereas the phase mode is described as uniform rotations of M_{xy}. Both of these modes have A_g symmetry, i.e., these are intrinsically Raman active because the continuous *rotational* symmetry is broken above H_c. This is one of the most distinguishing characteristics of the magnetic excitations in the magnon BEC phase. In systems of density waves,[24] the Goldstone mode (phase mode), which corresponds to the continuous *translational* operation, is IR active.

Let us show that the phase mode does not give the finite Raman intensity. When the phase mode is the Goldstone mode, i.e., for $E_{g+}(\boldsymbol{Q})=0$, $\mathcal{H}_{\pm}$ can be diagonalized by

$$\begin{pmatrix} \epsilon_{Q+} & -\Delta_{Q+} & \epsilon_{Q\pm} & -\Delta_{Q\pm} \\ \Delta_{Q+} & -\epsilon_{Q+} & \Delta_{Q\pm} & -\epsilon_{Q\pm} \\ \epsilon_{Q\pm} & -\Delta_{Q\pm} & \epsilon_{Q-} & -\Delta_{Q-} \\ \Delta_{Q\pm} & -\epsilon_{Q\pm} & \Delta_{Q-} & -\epsilon_{Q-} \end{pmatrix} \begin{pmatrix} u^{+}_{Q+} \\ v^{+}_{Q+} \\ u^{+}_{Q-} \\ v^{+}_{Q-} \end{pmatrix} = 0, \tag{8}$$

where the definitions of $\epsilon_{Q\beta}$ and $\Delta_{Q\beta}$ $(\beta=+,-,\pm)$ are given in Ref. 8. We can reduce Eq. (8) to the form of

$$\begin{pmatrix} \epsilon_{Q+} + \Delta_{Q+} & \epsilon_{Q\pm} + \Delta_{Q\pm} \\ \epsilon_{Q\pm} + \Delta_{Q\pm} & \epsilon_{Q-} + \Delta_{Q-} \end{pmatrix} \begin{pmatrix} u^{+}_{Q+} - v^{+}_{Q+} \\ u^{+}_{Q-} - v^{+}_{Q-} \end{pmatrix} = 0. \tag{9}$$

Because the matrix in Eq. (9) is invertible, we find that $u^{+}_{Q+} - v^{+}_{Q+} = 0$, i.e., the Raman intensity for the phase mode is zero although this mode is symmetrically allowed. This result indicates that only the spin correlation function along x is detectable with a factor M^2_{xy} by the first-order Raman scattering.

In the case of $TlCuCl_3$, the anisotropic exchange interaction gives a small magnetic gap $E_{g+}(\boldsymbol{Q}) \approx 1.7\ \text{cm}^{-1}$.[10] In this case, the $E_{g+}(\boldsymbol{Q})$ mode is the mixed amplitude and phase modes and it gives a finite one-magnon Raman intensity. In our measurements, however, we could not detect it because of the strong direct scattering at 0 cm^{-1}. It is worthwhile to consider the Raman scattering from the $E_{g+}(\boldsymbol{Q})$ mode because this mode is thermally populated at 1.9 K. The transition to the ground state is the one-magnon anti-Stokes Raman scattering, which cannot be detected in our measurements, as stated above. The transition to the $E_{g-}(\boldsymbol{Q})$ mode is obtained from the terms $\alpha^{-\dagger}_{k}\alpha^{+}_{k}$ in Raman tensor. Substituting $\alpha^{\pm}_{k}$ and $\alpha^{\pm\dagger}_{k}$ in Eq. (6) for $b_{k\pm}$ and $b^{\dagger}_{k\pm}$ in Eq. (5), $\mathcal{R}_{d}$ contains the terms

$$\sum_{k} \left\{ \frac{1}{4}(u^{+*}_{-k+}u^{-}_{-k+} + v^{+*}_{-k+}v^{-}_{-k+} + u^{+*}_{-k-}u^{-}_{-k-} + v^{+*}_{-k-}v^{-}_{-k-}) - v^{2}(u^{+*}_{-k+}u^{-}_{-k+} + v^{+*}_{-k+}v^{-}_{-k+}) \right\} \alpha^{-\dagger}_{k}\alpha^{+}_{k}. \tag{10}$$

This result indicates that the transition from the $E_{g+}(\boldsymbol{Q})$ state to the $E_{g-}(\boldsymbol{Q})$ one may be detected as a part of the two-magnon Raman band and its intensity is expected to have no drastic change, at least below 10 T, because v^2 below 10 T is very small.[8,16] Actually, the profile and intensity of the two-magnon Raman band at 9 T are almost similar to those at 0 T, as shown in Fig. 1.

When we consider one-magnon Raman scattering caused by the interdimer interaction, we can substitute the expectation value for one of the spin operators in Eq. (2),

$$\mathcal{R} = \sum_{i,j} F_{i,j}(\hat{\boldsymbol{E}}_{\text{in}} \cdot \hat{\boldsymbol{r}}_{ij})(\hat{\boldsymbol{E}}_{\text{sc}} \cdot \hat{\boldsymbol{r}}_{ij})\boldsymbol{S}_{i} \cdot \langle \boldsymbol{S}_{j} \rangle. \tag{11}$$

The Raman tensor from the interdimer interaction also contains the terms $(b_{Q+} + b^{\dagger}_{Q+})$, suggesting that the one-magnon Raman scattering from the $E_{g-}(\boldsymbol{Q})$ mode can be detected above H_c. Because $\langle S \rangle = M_{xy}$, one can expect that the Raman intensity is also proportional to M^2_{xy}. The precise analytic form of the Raman tensor coming from the interdimer interaction has been established in our recent letter in the case of the pressure-induced magnon BEC phase at zero magnetic

field.[25] The magnetic field induced magnon BEC case will be published elsewhere.[26]

We point out that our theory for the appearance of the one-magnon Raman scattering is applicable to the pressure-induced magnon BEC phase transition in $TlCuCl_3$.[8,27,28] In the case of pressure-induced magnon BEC phase transition, the pure amplitude mode, which is the longitudinal spin-wave mode coupled only with the spin correlation function along the x direction in Fig. 4, is expected to be observed.[25,29]

The two-magnon Raman band is also interesting as well as the appearance of the one-magnon Raman peak which is the main purpose of this paper. In the case of two-magnon Raman scattering, both $\mathcal{R}_d$ and the Raman tensors generated from the interdimer interactions, which create the magnon pair with the zero total momentum, play an essential role. At present, it is difficult to calculate the line shape of the two-magnon Raman band because the values of $F_{i,j}$, to which the two-magnon Raman spectrum is sensitive, cannot be directly obtained.

V. CONCLUSION

We have assigned the origin of the Raman peak appearing above H_c in $TlCuCl_3$ to one-magnon Raman scattering, which comes from the exchange magnon Raman process. This is based on (1) the Lorentzian line shape of the peak, (2) its Raman shift tracing $E_{g-}(\boldsymbol{Q})$, (3) its polarization characteristics, i.e., this one-magnon Raman scattering is A_g symmetric as well as the second-order magnetic Raman scattering, and (4) the observation that the peak's Raman intensity is proportional to M_{xy}^2. By using the bond-operator representation, we calculated the Raman intensity to clarify the Raman selection rule of one-magnon Raman scattering in the exchange magnon Raman process. The intensity of the one-magnon Raman scattering is related to the spin correlation function along the direction of M_{xy}, i.e., the x direction in Fig. 4. Therefore, the $E_{g\pm}(\boldsymbol{Q})$ modes with the finite excitation energies are A_g symmetric and Raman active. In the isotropic limit, the Goldstone mode for $E_{g+}(\boldsymbol{Q})=0$, which is related to the spin correlation function along the y direction, is A_g symmetric but has no Raman intensity. The $E_{g0}(\boldsymbol{Q})$ mode and the magnetic excitation at the chemical Γ point are Raman inactive. The change of the ground and excited states through the magnon BEC phase transition can be detected via the appearance of a one-magnon Raman peak from the $E_{g-}(\boldsymbol{Q})$ mode in the magnon BEC phase.

*kuroe@sophia.ac.jp

[1] A. Oosawa, M. Ishii, and H. Tanaka, J. Phys.: Condens. Matter **11**, 265 (1999).
[2] T. Nikuni, M. Oshikawa, A. Oosawa, and H. Tanaka, Phys. Rev. Lett. **84**, 5868 (2000).
[3] H. Tanaka, A. Oosawa, T. Kato, H. Uekusa, Y. Ohashi, K. Kakurai, and A. Hoser, J. Phys. Soc. Jpn. **70**, 939 (2001).
[4] F. Yamada, T. Ono, H. Tanaka, G. Misguich, M. Oshikawa, and T. Sakakibara, J. Phys. Soc. Jpn. **77**, 013701 (2008).
[5] M. Jaime, V. F. Correa, N. Harrison, C. D. Batista, N. Kawashima, Y. Kazuma, G. A. Jorge, R. Stein, I. Heinmaa, S. A. Zvyagin, Y. Sasago, and K. Uchinokura, Phys. Rev. Lett. **93**, 087203 (2004).
[6] T. Waki, Y. Morimoto, C. Michioka, M. Kato, H. Kageyama, K. Yoshimura, S. Nakatsuji, O. Sakai, Y. Maeno, H. Mitamura, and T. Goto, J. Phys. Soc. Jpn. **73**, 3435 (2004).
[7] C. Rüegg, N. Cavadini, H.-U. Güdel, K. Krämer, H. Mutka, A. Wildes, K. Habicht, and P. Vorderwisch, Nature (London) **423**, 62 (2003).
[8] M. Matsumoto, B. Normand, T. M. Rice, and M. Sigrist, Phys. Rev. B **69**, 054423 (2004).
[9] P. A. Fleury and R. Loudon, Phys. Rev. **166**, 514 (1968).
[10] V. N. Glazkov, A. I. Smirnov, H. Tanaka, and A. Oosawa, Phys. Rev. B **69**, 184410 (2004).
[11] K. Kusakabe, H. Kuroe, A. Oosawa, T. Sekine, M. Fujisawa, and H. Tanaka, J. Magn. Magn. Mater. **310**, 1365 (2007).
[12] K.-Y. Choi, G. Güntherodt, A. Oosawa, H. Tanaka, and P. Lemmens, Phys. Rev. B **68**, 174412 (2003).
[13] T. Sekine, M. Jouanne, C. Julien, and M. Balkanski, Phys. Rev. B **42**, 8382 (1990).
[14] H. Kuroe, J. I. Sasaki, T. Sekine, N. Koide, Y. Sasago, K. Uchinokura, and M. Hase, Phys. Rev. B **55**, 409 (1997).
[15] J. W. Halley, Phys. Rev. Lett. **41**, 1605 (1978).
[16] M. Matsumoto, B. Normand, T. M. Rice, and M. Sigrist, Phys. Rev. Lett. **89**, 077203 (2002).
[17] A. Oosawa, T. Kato, H. Tanaka, K. Kakurai, M. Müller, and H.-J. Mikeska, Phys. Rev. B **65**, 094426 (2002).
[18] K. Takatsu, W. Shiramura, and H. Tanaka, J. Phys. Soc. Jpn. **66**, 1611 (1997).
[19] W. H. Weber and G. W. Ford, Phys. Rev. B **40**, 6890 (1989).
[20] P. Knoll, C. Thomsen, M. Cardona, and P. Murugaraj, Phys. Rev. B **42**, 4842 (1990).
[21] T. Sekine, H. Kuroe, J. Sasaki, Y. Sasago, N. Koide, K. Uchinokura, and M. Hase, J. Phys. Soc. Jpn. **67**, 1440 (1998).
[22] G. Els, P. H. M. van Loosdrecht, P. Lemmens, H. Vonberg, G. Güntherodt, G. S. Uhrig, O. Fujita, J. Akimitsu, G. Dhalenne, and A. Revcolevschi, Phys. Rev. Lett. **79**, 5138 (1997).
[23] K.-Y. Choi, A. Oosawa, H. Tanaka, and P. Lemmens, Phys. Rev. B **72**, 024451 (2005).
[24] G. Grüner, *Density Waves in Solids* (Addison-Wesley, Reading, MA, 1994), Chap. 6.
[25] M. Matsumoto, H. Kuroe, A. Oosawa, and T. Sekine, J. Phys. Soc. Jpn. **77**, 033702 (2008).
[26] M. Matsumoto (unpublished).
[27] K. Goto, M. Fujisawa, T. Ono, H. Tanaka, and Y. Uwatoko, J. Phys. Soc. Jpn. **73**, 3254 (2004).
[28] A. Oosawa, M. Fujisawa, T. Osakabe, K. Kakurai, and H. Tanaka, J. Phys. Soc. Jpn. **72**, 1026 (2003).
[29] M. Matsumoto and M. Koga, J. Phys. Soc. Jpn. **76**, 073709 (2007).